Atmos. Chem. Phys. Discuss., 15, 19447–19476, 2015
www.atmos-chem-phys-discuss.net/15/19447/2015/
doi:10.5194/acpd-15-19447-2015

Atmospheric Chemistry and Physics Discussions

The contrasting roles of water and dust in controlling daily variations in radiative heating of the summertime Saharan Heat Low

J. H. Marsham[1,2], D. J. Parker[2], M. C. Todd[3], J. R. Banks[4], H. E. Brindley[4], L. Garcia-Carreras[2], A. J. Roberts[2], and C. L. Ryder[5]

[1]National Centre for Atmospheric Science (NCAS), UK
[2]water@leeds, School of Earth and Environment, University of Leeds, Leeds, UK
[3]Department of Geography, University of Sussex, Brighton, UK
[4]Space and Atmospheric Physics Group, The Blackett Laboratory, Imperial College, London, UK
[5]Department of Meteorology, University of Reading, Reading, UK

Received: 13 May 2015 – Accepted: 1 June 2015 – Published: 16 July 2015

Correspondence to: J. H. Marsham (j.marsham@leeds.ac.uk)

Published by Copernicus Publications on behalf of the European Geosciences Union.

Abstract

The summertime Sahara Heat Low (SHL) is a key component of the West African Monsoon (WAM) system. Considerable uncertainty remains over the relative roles of water vapour and dust aerosols in controlling the radiation budget over the Sahara and therefore our ability to explain variability and trends in the SHL, and in turn, the WAM. Here, new observations from the Fennec field campaign during June 2011 and June 2012, together with satellite retrievals from GERB, are used to quantify how total column water vapour (TCWV) and dust aerosols (from aerosol optical depth, AOD) control day-to-day variations in energy balance in both observations and ECWMF reanalyses (ERA-I). The data show that the earth-atmosphere system is radiatively heated in June 2011 and 2012. It is TCWV that largely determines variations in daily mean TOA net flux and the net heating of the earth-atmosphere system. In contrast, dust provides the primary control on surface heating, but the decreased surface heating from dust is largely compensated by increased atmospheric heating, and so dust control on net TOA radiation is weak. Dust and TCWV are both important for direct atmospheric heating. ERA-I captures the control of TOA net flux by TCWV, with a positive correlation ($r = 0.6$) between observed and modelled TOA net radiation, despite the use of a monthly dust climatology in ERA-I that cannot capture the daily variations in dustiness. Variations in surface net radiation, and so the vertical profile of radiative heating, are not captured in ERA-I, since it does not capture variations in dust. Results show that ventilation of the SHL by cool moist air leads to a radiative warming, stabilising the SHL with respect to such perturbations. It is known that models struggle to capture the advective moistening of the SHL, especially that associated with mesoscale convective systems. Our results show that the typical model errors in Saharan water vapour will lead to substantial errors in the modelled TOA energy balance (tens of $W\,m^{-2}$), which will lead to errors in both the SHL and the WAM.

ACPD
15, 19447–19476, 2015

1 Introduction

The Sahara lies under the descending branch of the Hadley circulation and during summer the intense solar heating combined with the arid environment leads to large sensible surface heat fluxes and the formation the Saharan Heat Low (SHL). This increases the pressure gradient from the Gulf of Guinea to the Sahara, driving the West African Monsoon (WAM), and variations in the SHL modify the WAM on time scales from days to decades (Thorncroft and Blackburn, 1999; Peyrillé and Lafore, 2007; Biasutti et al., 2009; Lavaysse et al., 2009, 2010; Chauvin et al., 2010; Xue et al., 2010; Martin and Thorncroft, 2014; Martin et al., 2014). There is a shortage of routine observations in the SHL and substantial disagreements exist even between analyses (Marsham et al., 2011; Roberts et al., 2014). The Fennec project aimed to better quantify processes governing the Saharan atmosphere (Washington et al., 2012; Ryder et al., 2015) and deployed an observational supersite-1 close to the climatological centre of the SHL (Marsham et al., 2013a).

The radiative budget of the Sahara is significantly modulated by variations in clouds, dust and water vapour. Charney (1975) shows how the high albedo and dry atmosphere can lead to a top-of-atmosphere (TOA) net radiative cooling in July, with heating via subsidence, proposing a positive feedback where dry soils with little vegetation generate high albedo, favouring atmospheric descent and low rainfall. The dry atmosphere means that water vapour provides a key control in the longwave with vapour at all levels affecting top-of-atmosphere (TOA) outgoing longwave (Allan et al., 1999; Brindley and Harries, 1998). Evan et al. (2015) suggest that the increasing temperatures within the SHL over the past 30 years, key to the recovery of the Sahel from drought, are driven by longwave impacts of increasing water vapour, in the "Saharan Water Temperature" feedback. Shallow clouds on top of the deep dry boundary layer (Cuesta et al., 2009) occur around 20 % of the time over the Sahara, with mid-level clouds reducing net surface shortwave and increasing net surface longwave in the Sahel (Stein et al., 2011; Bouniol et al., 2011). Dust absorbs and emits longwave radiation (Haywood et

ACPD
15, 19447–19476, 2015

al., 2005) and scatters and absorbs shortwave (Ryder et al., 2013; Banks et al., 2014). At the TOA, and over the bright Sahara, dust induces a warming as its longwave effects dominate its shortwave effects (Balkanski et al., 2007; Yang et al., 2009). Operational, global models use either prognostic dust or dust climatologies, but struggle to capture variations in summertime dust, partly as cold-pool outflows from convection (haboobs) provide a key uplift mechanism that is missing in global models (Marsham et al., 2011, 2013a; Heinold et al., 2013).

At low levels the Sahara is cooled by advection from neighbouring moister and cooler regions, including the WAM to the south. Representing the monsoon is a challenge to models, partly because of the representation of convection, in particular its diurnal timing and cold pools; the diurnal timing of Sahelian moist convection affects the pressure gradient driving the monsoon, modulating the flux of water vapour from the Sahel to the Sahara and hence rainfall over the Sahel (Marsham et al., 2013b; Birch et al., 2014). Furthermore cold pools form a significant component of the monsoon (Marsham et al., 2013b) and also ventilate the Sahara from the Atlas in the north (Emmel et al., 2010); most temperature and humidity biases in the Met Office global model at the Fennec supersite-1 during June 2011 were caused by missing cold pool advection (Garcia-Carreras et al., 2013). Similarly ventilation of the Sahara by the Atlantic Inflow involves mesoscale flows that are a challenge for global models (Grams et al., 2010; Todd et al., 2013). Since clouds, water vapour and dust are all important to the Sahara's radiative energy balance, such model errors in convection, clouds, haboobs and advection of water vapour will all affect modelled radiative energy balances and hence climate.

There is a clear need to establish the controls on the radiation budget over the Sahara and evaluate models. In this paper we use observations of surface radiative fluxes from Fennec and retrievals of TOA fluxes from satellite data to investigate how dust and water control the day-to-day variations in energy balance over the Fennec supersite-1 in the summertime SHL region, and how this is represented in ERA-Interim (ERA-I) reanalysis. Section 2 describes methods, Sect. 3 presents results, Sect. 4 contains discussion and conclusions are in Sect. 5.

ACPD
15, 19447–19476, 2015

2 Method

We use data from Fennec supersite-1 in the central Sahara, located at Bordj-Badji Mokhtar (BBM) at 21.4° N 0.9° E, close to the SHL's climatological centre and the dust maximum (Marsham et al., 2013a), together with corresponding values from ERA-Interim (Dee et al., 2011), and satellite TOA fluxes (Harries et al., 2005; Dewitte et al., 2008). These satellite TOA fluxes are produced using a narrow to broad band conversion of SEVIRI (Spinning Enhanced Visible and Infrared Imager) radiance measurements. These are scaled by co-located GERB measurements and converted into broadband fluxes measurements at a horizontal resolution of 3 × 3 SEVIRI pixels (0.32–4 microns in the shortwave, and 4–100 microns in the longwave). This enhancement gives a spatial resolution of 9 km at nadir, compared with the 45 km of the native GERB. These observed fluxes are from clear and cloudy skies, but we also use the European Organisation for the Exploitation of Meteorological Satellites' MPEF (Meteorological Product Extraction Facility) cloud mask as a simple measure of cloud cover.

Fennec data are from intensive observation periods (IOPs) in June 2011 and 2012, when a Cimel sun photometer provided Aerosol Optical Depths (AODs) at 675 nm, a Kipp & Zonen radiometer mounted at 2 m provided measurements of broad-band radiative fluxes and 3 to 6-hourly radiosonde observations were available (Marsham et al., 2013a). The sun-photometer is part of the AERONET program (Holben et al., 1998) and cloud-screened AOD retrievals are only available during the day. Level-2 AOD data are not available for 2012 since not all data meet level-2 requirements. However, the 0.675 nm AODs are still reliable. We therefore use level-2 data for 2011 and level-1.5 for 2012, noting that using only 2011 data does not affect our conclusions. We use the radiosondes to compute column water vapour from the surface to 300 hPa (a height consistently reached by the radiosondes), which we refer to simply as "total column water vapour (TCWV)". During June 2011 BBM was regularly cooled by nocturnal monsoon flows and embedded cold pools giving substantial variability in TCWV

ACPD
15, 19447–19476, 2015

(Marsham et al., 2013a), and qualitatively similar weather events were observed during June 2012.

In order to study the day-to-day variations in the energy budget, we average all data to their daily means. Complete surface flux data were only available for 13 days in June 2011 (9, 10, 18–20, 23–27, 30 June) and 25 days in June 2012 (all except 3, 16–18, 30 June). Some dates had short data gaps (around two hours on two days, but otherwise an hour or less) and these gaps were interpolated across in order to include 7, 17, 21, 22 June 2011 and 16–17 June 2012. This gave an improved range of AODs, albeit with increased uncertainties in surface fluxes. Fluxes from these days with some interpolation are marked by asterisks in Figs. 1 to 4, and the effects of interpolation are discussed in Sect. 3, where it is seen that results from these days are physically consistent with other data from days without interpolation. The surface flux data from Kipp and Zonen radiometers have slightly different spectral ranges to the satellite-borne GERB: Kipp and Zonen are 0.3 to 2.8 µm in the shortwave and 4.5 to 42 µm in the longwave, whilst GERB is 0.32 to 4 µm and 4 to 100 µm. This means that the surface-based Kipp and Zonen can miss up to 3.5 $W m^{-2}$ net shortwave atmospheric heating as would be seen by GERB and up to 3.8 $W m^{-2}$ of the net longwave as would be seen by GERB (Banks et al., 2014). This introduces errors of up to around 3 $W m^{-2}$ in our inferred direct atmospheric radiative heating rates, but does not affect our analysis and conclusions, which is focused on the controls on the variability of these rates, rather than their absolute values.

Sun-photometer AODs were available from 8 June 2011 (with no observations on 13 June) and 1 to 28 June 2012 (with no observations on 17–19 June). Radiosondes were available from 8 June 2011 and 1 to 26 June 2012. The number of observations contributing to the daily mean is variable for AODs, since observations are only made when it is cloud free, but all days except one had at least eight AOD observations and the daily-mean AOD range of 0.2 to 2.7 is similar to that of the observation range in AODs (0.2 to 3.9) and the diurnal cycle in AOD is weak (Marsham et al., 2013a; Banks

ACPD
15, 19447–19476, 2015

et al., 2014). Overall this gave 36 days with surface data, observed AOD and observed TCWV and 44 days with TCWV and AOD.

3 Results

In order to determine the relative importance of TCWV and dust for the radiation budget we analyse relationships between the daily means of key variables, using both observed quantities and the equivalent from ERA-I at the location of BBM. ERA-I uses a climatological AOD field and so cannot capture the observed daily variability in AOD. This, in effect, represents a quasi-control experiment for dust variability. All correlations and regression trends discussed are listed in Table 1 (correlations in bold are significant at the 90 % level). Relationships are shown using days where surface data are available ("Good surface data"), and for all available data ("All data") where surface flux data are not required. The trends are very similar whichever dataset is used and values in the text are for "Good surface data", unless otherwise noted. The effect of subsampling is small for ERA-I, showing that general lessons can be drawn from the observational data, despite the limited time-span of the dataset.

Figure 1a shows that there is a significant tendency for more dust with more TCWV, although there are a few dry dusty days (correlation = 0.29). The use of surface flux data with some interpolation (shown by asterisks) allows study of more days with high AODs. The mechanisms underlying this correlation are understood: Marsham et al. (2013a) shows how moist monsoon surges from the south are associated with dust at BBM. This is because the moist surges are associated with both dusty haboobs and moist nocturnal low-level jets (LLJs) that together dominate the dust uplift at BBM in June 2011 (Marsham et al., 2013a; Allen et al., 2013). The association between dust and water vapour, is consistent with Fig. 16 in Marsham et al. (2013a), which shows a statistical link between AOD and cloud cover at BBM. Intense dust uplift does occur in dry air, however, especially in the dry Harmattan LLJs (Marsham et al., 2013a; Allen et al., 2013).

ACPD
15, 19447–19476, 2015

A principal components analysis (PCA) was performed on net surface and TOA fluxes, AOD and TCWV for the daily totals for the 36 days where data were available, standardising each variable to mean = 0, variance = 1. Principal components do not have to correspond to "physical modes", but are each orthogonal, with each component having the largest possible variance given that it is orthogonal to preceding components (and the first mode having maximum possible variance). In this case, the first principal component explains 53 % of the variance and has an eigenvector of −0.75 (for TCWV), −0.77 (AOD), 0.63 (net surface flux), −0.76 (net TOA flux), i.e. TCWV and AOD correlate (as discussed above) with increased TCWV and AOD together reducing net surface flux and increasing net TOA flux. The reasons for these impacts on fluxes are discussed in following sections, but we note here the impacts are consistent with: (i) water vapour, clouds and dust giving a net TOA longwave warming, and (ii) dust and cloud giving a net surface cooling due to their shortwave effects. The second principal component explains 34 % of the variance with an eigenvector of −0.56 (for TCWV), 0.51 (AOD), −0.69 (net surface flux), −0.54(net TOA flux), i.e. TCWV anti-correlated with AOD, with increased TCWV increasing net TOA flux and, simultaneously, decreasing AOD increasing net surface flux. We return to the physical interpretation of this PCA in subsequent analysis.

3.1 Control of TOA net radiation by water (TCWV) and aerosols (AOD)

Daily mean net TOA radiation is always positive (i.e. downwards) and has a mean value of 26 W m^{-2}, i.e. there is warming of the earth-atmosphere system throughout the period (Fig. 2a). Net heating varies between around 0 and 70 W m^{-2}, or approximately 0 to 1.2 K day^{-1} if the heating were distributed over the 5 km deep boundary layer.

There is a significant correlation of 0.74 between TCWV and TOA net radiation. Figure 2a shows that water vapour warms the atmosphere, with a trend in TOA net radiation with TCWV of +2.2 W kg^{-1}. This is a result of a 3.2 W kg^{-1} increase in TOA net longwave with TCWV in observations (Fig. 2d), from water vapour, clouds (and associated dust) reducing TOA outgoing longwave. This longwave TCWV effect dominates

ACPD
15, 19447–19476, 2015

the decrease in net shortwave with increased water vapour ($-0.98\,W\,kg^{-1}$, Fig. 2g), due to water vapour and associated clouds and dust. The correlations are strongest between TCWV and TOA net or longwave radiation (both 0.74 and 0.68), rather than TOA shortwave (−0.36), presumably since the water vapour directly affects the longwave, while the much of the shortwave effects of TCWV are indirect, occurring via associated clouds and dust.

The correlation between AOD and TOA net radiation (Fig. 2b) is much weaker than between TCWV and TOA net radiation (0.26 compared with 0.74). Figure 2b shows that TOA net radiation increases with AOD ($5.3\,W\,m^{-2}$ per AOD, comparable with Balkanski et al., 2007), but this relationship is complex and its magnitude decreases to $3.5\,W\,m^{-2}$ if all available data are used (with a correlation of 0.17). The increase in net TOA radiation with AOD occurs because the trend in TOA longwave ($+10.5\,W\,m^{-2}$ per AOD) dominates the TOA net shortwave ($-5.2\,W\,m^{-2}$ per AOD; Fig. 2e and h). The observed net effect of dust at TOA and the dominance of the longwave for this effect are both consistent with previous studies (Balkanski et al., 2007; Yang et al., 2009). Banks et al. (2014) show that in clear-sky the diurnal mean effect of dust at BBM is warming in the shortwave. Therefore the observed shortwave cooling associated with dust reported in Fig. 2 is likely a result of cross correlation of AOD and cloud. This cloud, as well as the water vapour and dust, reduces outgoing longwave, leading to a warming. The effects of AOD and TCWV variations on radiation normalised by the standard deviation (σ) in either AOD or TCWV (Table 1, values in square brackets) show that the variance in TCWV has a much larger effect on TOA net radiation ($10.4\,W\,m^{-2}$ per σ) than the variance in AOD ($3.6\,W\,m^{-2}$ per σ, or $2.3\,W\,m^{-2}$ if "All data" are used), i.e. most day-to-day variations in net TOA radiation are mostly controlled by TCWV, not AOD.

Figure 1b shows daily net shortwave heating is always greater than net longwave cooling (the Earth-atmosphere system is warming in June). Daily variations in shortwave are anti-correlated with variations in longwave such that as daily net TOA shortwave decreases, the net longwave increases (correlation of −0.80). In Fig. 1b, if the

ACPD
15, 19447–19476, 2015

gradient is less than −1, reducing the net shortwave will increase the net flux. The observed gradient is −1.4, i.e. decreased shortwave tends to lead to an increase in net heating due to the corresponding greater increase in longwave (i.e. reduced LW cooling). As such, TOA daily variability at BBM is influenced more by variability in the longwave than the shortwave.

TCWV and aerosol effects at TOA in ERA-I

The ERA-I trends in TOA net radiation with TCWV of 1.3 W kg^{-1} (1.4 W kg^{-1} for all data) is similar to that observed (2.2 W kg^{-1}, 2.1 W kg^{-1} for all data, Fig. 2c and a). ERA-I captures the trends in both TOA net longwave and shortwave with TCWV, although it underestimates both (1.8 W kg^{-1} in longwave for ERA-I, compared with the 3.2 W kg^{-1} observed, and −0.48 W kg^{-1} in shortwave for ERA-I compared with the −0.98 W kg^{-1} observed; Fig. 2f and i). As observed, reduced net shortwave increases TOA net flux in ERA-I (Fig. 1c, gradient of −1.4).

Even though it does not account for the daily variations in dust, ERA-I captures much of the day-to-day variations in TOA net variation (correlations with observations are 0.62 and 0.73 for "All data" and "Good surface data", not shown). Table 1 shows the regressed trends in ERA-I fluxes with observed AODs. These trends are of the correct sign: this suggests that some of the observed trends with AOD are due to associated water vapour and cloud (captured at least to some extent by ERA-I), rather than dust. This is consistent with the lower correlations between observed AOD and observed TOA net flux (0.26) than between observed TCWV and observed TOA net flux (0.74), discussed in the previous section.

The differences in the effects of TCWV in ERA-I and in observations are likely because of both errors in clouds in ERA-I and its lack of variability in dust. Detailed validation of model clouds over the bright dusty Sahara is challenging and beyond the scope of this paper. Here, we note that ERA captures day-to-day variations of mean cloud fraction (correlation with MPEF cloud mask of 0.56), but mean cloud fraction in ERA-I is 0.22, much less than the MPEF value of 0.53, although this value is likely biased

ACPD
15, 19447–19476, 2015

high by dust. Surface albedo in ERA-I is very close to observed, but TOA upward shortwave in ERA-I is about 15 W m^{-2} less than in observations (although daily maxima in these values are similar, not shown). These comparisons with data both support the hypothesis that ERA-I underestimates cloud cover. The underestimate of the longwave effect of TCWV at TOA in ERA-I is consistent with this suspected underestimation of cloud cover in ERA-I and also the lack of dust associated with TCWV reducing outgoing longwave (Haywood et al., 2005). However, in ERA-I the underestimation of the magnitude of the trends in TOA net longwave with TCWV (1.8 compared with 3.2 W kg^{-1}) and shortwave with TCWV (−0.48 compared with −0.98 W m^{-2}) compensate to some extent give a trend in TOA net radiation with TCWV of 1.3 W kg^{-1} in ERA-I, close to the 2.2 W kg^{-1} observed.

3.2 Control of surface net radiation by TCWV and AOD

At the surface AOD provides a strong control on net radiation (Fig. 3b) with a significant trend of −13.1 W m^{-2} per AOD. This is a result of compensating longwave and shortwave effects, with the shortwave effect being largest: Fig. 3h shows −31.9 W m^{-2} surface net shortwave per AOD, with dust reducing solar heating at the surface (largely compensated by heating the atmosphere above, comparing with −5.2 W m^{-2} TOA net shortwave per AOD, Sect. 3.3). Figure 3e shows +20.7 W m^{-2} surface net longwave per AOD, i.e. dust, together with the water vapour and cloud associated with the dust, warms the surface in the longwave, but unlike at TOA this does not compensate fully for the shortwave effects. The effects of AOD on net, shortwave and longwave fluxes are consistent between the days with some interpolated values (asterisks) and other days (pluses).

TCWV decreases surface net radiation by 0.20 W kg^{-1}. This is a balance of +2.0 W kg^{-1} from the longwave and −1.8 W kg^{-1} from the shortwave i.e. is a small difference between two large numbers. Impacts of TCWV on surface net heating are therefore a subtle balance of water vapour, clouds and associated dust. If variations in surface net radiation with AOD and TCWV are normalised by the standard deviation

ACPD
15, 19447–19476, 2015

in AOD or TCWV, variability in AOD is seen to dominate the variations in surface net radiation (square brackets in Table 1). For the impacts of TCWV, the days with some interpolated values at first appear to be inconsistent with other days (Fig. 2a, d, g), but this is due to the high AODs for these days, the effects of which are consistent with other data (Fig. 3b, e, h).

At the surface, although the observed shortwave and longwave variations are anti-correlated (coefficient = −0.88), they cancel to a much lesser extent than at TOA. Figure 1d shows how decreased shortwave leads to increased net longwave, but this does not tend to compensate fully (gradient of −0.61), so decreased shortwaves gives decreased net surface radiation. As such, daily variability in surface net radiation at BBM is influenced more by variability in the shortwave than the longwave. Again data from days with some interpolation of surface fluxes (asterisks) are consistent with other days (pluses).

The analysis of TOA and net fluxes in Sects. 3.1 and 3.2 is consistent with the PCA in Sect. 3. Increasing and co-varying dust and TCWV reduce net surface flux (mode 1) and increase TOA net flux, explaining 53 % of the data variance (mode 1). A further 34 % of variance is explained by TCWV anti-correlated with AOD (mode 2), with increased TCWV increasing TOA net flux and decreased AOD increasing net surface flux.

Effects of TCWV and AOD at the surface in ERA-I

Figure 3c shows that, in contrast with observations (Fig. 3a), ERA-I always produces an *increase* in net surface radiation with increasing TCWV ($+0.76\,W\,kg^{-1}$, compared with $-0.20\,W\,kg^{-1}$). Figure 1e shows that at the surface in ERA-I, unlike in observations, decreased net shortwave is always compensated by increased net longwave (gradient −1.1). This occurs since in ERA-I greater water vapour gives greater net surface longwave (Fig. 3f), without the associated dust to reduce the net surface shortwave (Fig. 3i): the net surface radiation in ERA-I depends largely on surface longwave, whereas in observations it depends largely on the shortwave. As a result, ERA-I, which uses a

ACPD
15, 19447–19476, 2015

monthly dust climatology, fails to capture day-to-day variations in surface net radiation, producing no correlation (0.02) with observations.

Although it does not affect the trends of surface fluxes with TCWV and AOD discussed above, we note here that ERA-I surface net longwave is on average 55 W m^{-2} less than observed, and this is almost all from more upward longwave than observed (not shown). Due to the non-linear nature of thermal emission, the 13 % error in upward longwave can be caused by only a 3 % error in skin temperature (or from an error in emissivity). Maximum values of daily ERA-I surface net shortwave are similar to observed, but minima are higher, likely from missing dust and cloud. These two errors lead to surface net radiation being around 34 W m^{-2} lower in ERA-I than observed.

3.3 Radiative heating of the atmosphere

The TOA and surface fluxes are differenced to give the radiative flux convergence within the atmosphere, i.e. the direct radiative heating of the atmosphere (Fig. 4). As expected the atmosphere is cooling in the longwave and is heated in the shortwave. There are statistically significant positive correlations between both TCWV or AOD (which are themselves correlated, Fig. 1a) and net radiative heating of the atmosphere (Fig. 4a and b). For AOD there is a strong correlation (0.93) with shortwave atmospheric heating (Fig. 4h, 26.7 W m^{-2} per AOD, comparable with Balkanski et al., 2007) that dominates the trend of net longwave heating with AOD (Fig. 4e, −10.2 W m^{-2}). There are significant positive trends in net shortwave and net longwave radiative heating of the atmosphere with increasing TCWV (Fig. 4d and g). The longwave trend (Fig. 4d) is much less clear than it is at TOA or at the surface, since the trends at TOA and the surface (Figs. 2d and 3d) are similar (3.2 and 2.0 Wm^{-2}) and largely cancel.

When trends with TCWV and AOD are normalised by the standard deviations in TCWV and AOD to allow comparison (results in square brackets in Table 1), effects of AOD dominate those from TCWV, but this is much more pronounced in the shortwave. The results therefore show significant shortwave heating of the atmosphere by dust (consistent with Banks et al., 2014), consistent with the large effect of AOD on surface

ACPD
15, 19447–19476, 2015

net and surface net shortwave fluxes, with much smaller effects at TOA. Decreases in surface heating from dust are largely compensated by direct radiative heating of the atmosphere. The increase in net longwave heating with TCWV is expected due to the warming from both water vapour and clouds. The shortwave heating from TCWV (correlation coefficient of only 0.19) is similar to that in ERA (Sect. 3.3.1) showing that is not just from associated dust, but from shortwave absorption by water (although points with unusually high shortwave heating are explained by AODs, Fig. 4g and h). Figure 1f shows how increasing longwave cooling of the atmosphere is more than compensated for by the corresponding increased shortwave heating (gradient = −0.39); atmospheric heating is largely controlled by effects of dust on the shortwave, whereas longwave atmospheric heating is much less variable.

Atmospheric heating in ERA-I

ERA gives weaker longwave atmospheric cooling than observed and therefore less net atmospheric cooling (Fig. 4c and f). Lacking the observed variability in dust, ERA has little variability in atmospheric shortwave heating, with almost no correlation of shortwave heating with observed AODs (Table 1). ERA has a significant positive trend in shortwave atmospheric heating with TCWV (Fig. 4i, 0.91 $W\,kg^{-1}$) from absorption by water (similar to that observed, Fig. 4g, 0.78 $W\,kg^{-1}$). While observations have a significant, but weak, positive correlation between TCWV and longwave atmospheric heating (Fig. 4d, 0.34), ERA has a weak insignificant negative correlation (Fig. 4f, −0.20). Trends are weak in both cases, since TOA and surface longwave fluxes both respond similarly to TCWV and ERA is of course lacking the variability in dust that correlates with TCWV and this may contribute to the difference. Despite the weak variation in shortwave atmospheric heating in ERA compared with observations, variations in shortwave dominate the trend in net atmospheric heating, giving increased net heating with increased TCWV (Fig. 4c). This trend is however much weaker than observed (Fig. 4a), since ERA has much less variability in net heating due to its use of a dust climatology.

ACPD
15, 19447–19476, 2015

4 Discussion

Since variability in water dominates day-to-day variability in net TOA heating it is crucial for models to capture the water content of the SHL. Small error in TCWV could cause errors in clear-sky longwave radiation comparable with the 50 $W\,m^{-2}$ from dust seen in Haywood et al. (2005). This paper shows that 50 $W\,m^{-2}$ TOA net longwave corresponds to around 16 $kg\,m^{-2}$ water (based on the 3.2 $W\,kg^{-1}$ dependence of TOA net longwave on TCWV, Table 1), roughly equivalent to 3 $g\,kg^{-1}$ over the 5 km deep boundary layer. Roberts et al. (2014) show that route-mean-square differences in *analyses* of WVMR at 20° N in the Sahara are around 1.5 $g\,kg^{-1}$, and show a case where differences between different analyses are around 4 $g\,kg^{-1}$. Garcia-Carreras et al. (2013) show a global model mean bias of around 1 $g\,kg^{-1}$ at Fennec supersite-1 in June 2011 in the model first guess (3-to-6 hour forecast), despite assimilation of the Fennec radiosoundings. Models struggle to capture monsoon flow that cools and moistens the SHL, in particular from cold pools (Marsham et al., 2013b; Garcia-Carreras et al., 2013). This study shows that errors in fluxes of water vapour will lead to a compensating error of insufficient radiative heating from the absence of the moister air. Model errors in dust will affect the vertical distribution of heating and so also affect vertical mixing and dynamics.

The results give some insight into the Saharan BL energy budget during June over BBM. We show TOA net radiative heating of around 26 $W\,m^{-2}$. There was an observed mean night-time cooling of around 4 K over an approximately 1 km depth every night (Marsham et al., 2013a), corresponding to around 50 $W\,m^{-2}$ cooling (not all of this cooling is advective, some is radiative). To compensate for this cooling an additional warming of around 20 $W\,m^{-2}$ is required. Daily entrainment of free-tropospheric air will raise the BL top, which is lowered by subsidence to give, in the long-term, a constant BL top. We can estimate the heating rate of the BL either from entrainment or subsidence. The 24 h entrainment flux is perhaps 10 $W\,m^{-2}$ (20 % of the 100 $W\,m^{-2}$ surface flux for 12 h). The 24 h subsidence of a lid of 5 K / 100 m with 0.1 $m\,s^{-1}$ is 5 $W\,m^{-2}$.

ACPD
15, 19447–19476, 2015

These simple estimates therefore leave a mis-match of around 10 W m^{-2}, but show that all terms (net daytime radiative warming, net night-time radiative and advective cooling, entrainment of warm subsiding air) are all of a similar order of magnitude and significant.

During monsoon surges in June 2011 BBM experienced sudden moistenings of upto around 5 g kg^{-1} (Fig. 5, Marsham et al., 2013a). If we assume that a value of 2.5 g kg^{-1} is more representative of the change over the 5 km deep Saharan BL (Fig. 3 in Marsham et al., 2013a, shows such monsoon surges tend to directly affect the lower of half of the 5 km layer) this gives a TOA net radiative heating of around 28 W m^{-2} (based a TCWV of 12.5 kg m^{-2} and a dependence of net radiation on TCWV of 2.2 W kg^{-1}, Table 1). If this heating is distributed over the 5 km deep Saharan BL it will result in a warming of around 0.5 K day^{-1}. It will therefore take days for the additional radiative warming to compensate for the cooling of a few degrees experienced in such events. This "radiative rewarming time scale" may be one contributing factor (together with time-scales such as those for advection & mixing time scales and synoptic features such as African Easterly waves) to the variability of the 3-to-30-day variability of the SHL observed by Lavaysse et al. (2010).

The observed net radiative heating of the SHL region observed at BBM during June appears to contrast with Charney (1975), which shows heating from subsidence and TOA cooling from radiation for the Sahara in July. However, the Fennec supersite-1 is at the northern limit of the ITD and regularly receives cold moist air from the south (Marsham et al., 2013a). Charney (1975) Fig. 1 shows net TOA heating at the location of the Fennec supersite in July, with TOA net cooling only north of around 22° N (interestingly the TOA heating extends northeastwards over the Hoggar mountains, a region that favours northward extent of moist monsoon air (Cuesta et al., 2010)). It is likely that further north away from the moistening from the monsoon the warmer drier atmosphere will give greater longwave cooling and a net radiative cooling, as shown by Charney (1975). This will be further investigated.

ACPD
15, 19447–19476, 2015

5 Conclusions

We have used unique observations of surface energy balance, TCWV and AOD from the central Sahara in June, together with retrievals from GERB, to investigate controls on the day-to-day variations in radiative heating in the SHL region. TOA fluxes show that on average the earth-atmosphere system is warming (26 W m^{-2}), the surface is warming (98 W m^{-2}) and the atmosphere is cooling (74 W m^{-2}), with the longwave cooling and the shortwave warming in each case. Although there are limits to the extent to which our empirical approach can disentangle the roles of dust, cloud and water vapour, largely due to correlations between these factors, the results provide new insight into their roles in controlling the radiative balance of the unique environment of the central Sahara (schematic in Fig. 5).

Water vapour and dust are observed to correlate in the central Sahara, likely due to the uplift of dust in monsoon surges and haboobs (Bou Karam et al., 2008; Marsham et al., 2008, 2013a). However, water vapour and not dust dominates day-to-day variability of TOA net radiation, and hence total heating of the earth-atmosphere system. ERA-I captures the observed variation in TOA net radiation (correlation with observations of around 0.65), despite a monthly dust climatology in ERA-I, which cannot capture day-to-day variations in dustiness. Variations in AOD dominate day-to-day variations in surface net radiation, which unsurprisingly are not captured in ERA-I.

At TOA, on average, decreased shortwave heating gives greater net heating due to associated increases in longwave heating. ERA-I captures this and the overall impact of TCWV on TOA net radiation, with a mean increase in TOA net radiation with TCWV of 1.3 W kg^{-1} compared with 2.2 W kg^{-1} in observations. There are, however, compensating errors in the effects of TOA net shortwave and longwave with TCWV in ERA-I. ERA-I under-estimates the effects of TCWV on both TOA longwave and shortwave: it misses corresponding variations in dust and although it captures much of the effects of water vapour, it likely underestimates cloud (and significant uncertainties in analysed

ACPD
15, 19447–19476, 2015

water vapour persist at BBM, even when radiosondes are assimilated, Garcia-Carreras et al., 2013).

At the surface, dust decreases net surface radiation in reality by around 13 $W m^{-2}$ per AOD. The effect of TCWV is weak, variable and a subtle balance between the competing effects of water vapour, clouds and dust ($-0.2 W kg^{-1}$). Unlike at the TOA, at the surface decreases in shortwave are on average not compensated by increases in longwave, leading to decreased net radiation with decreased shortwave. In contrast to the observations, ERA-I gives greater net surface radiation with decreased surface shortwave: it is missing the effects of varying dust and can only capture the effects of water and cloud, likely underestimating cloud. This gives no correlation between ERA-I surface net radiation and that observed and a mean heating of 98 $W m^{-2}$ compared with the observed value of 64 $W m^{-2}$, due to an overestimation of surface downward shortwave in ERA-I. Differences between TOA and surface fluxes are used to infer atmospheric radiative heating. Effects from TCWV on these are significant, but they are more strongly controlled by AODs, since dust has a much greater effect on surface net radiation than TOA net radiation, while effects of TCWV on TOA and surface heating are more similar.

The results show that, when the SHL is cooled by cold moist air from its margins, the overall effect is to increase net TOA radiative heating, rewarming the SHL, a feedback which stabilises the system, by rewarming the cool air. This occurs in both reality and ERA-I. This ventilation by cold air is, however, normally accompanied by clouds and dust, which together reduce surface net radiation, which is not captured by ERA-I, as ERA-I is missing the variations in dust (and likely under-predicts cloudiness). As a result, even if ERA-I gives the correct TOA net radiation in response to water vapour, it fails to distribute this heating correctly in the vertical, with too much surface heating and insufficient boundary-layer heating. This will destabilise the boundary-layer profile compared with reality, affecting subsequent modelled dry and moist convection and therefore modelled transport of heat, momentum, water vapour and dust.

ACPD
15, 19447–19476, 2015

Improved modelling of the energy budget of the SHL region is needed in models to improve predictions of the WAM across time scales (e.g. Evan et al., 2015). The results show that is important that models used for predictions can accurately capture the processes controlling the water vapour distribution over the Sahara, as well as the dust. This capability is currently questionable for both water (Marsham et al., 2013b; Birch et al., 2014; Garcia-Carreras et al., 2013; Roberts et al., 2014) and dust (Evan et al., 2014), with many dust errors coming from moist convection (Marsham et al., 2011; Heinold et al., 2013). The results presented here therefore strongly motivate the need to improve the representation of advection of water vapour, clouds and convection in models.

Acknowledgements. Fennec was funded by a NERC consortium grant (NE/G017166/1). We would like to thank Azzendine Saci, Abdelkader Ouladichir, Bouzianne Ouchene, Mohammed Salah-Ferroudj, Benyakoub Abderrahmane, Mohammmed Limam, and Diali Sidali (ONM) and Richard Washington (University of Oxford) for their contributions to setting up running the Fennec supersite, and indeed all at ONM Algeria for their patience and hospitality during Fennec. We would like to thank the AERONET PHOTONS team for their assistance with the Cimel Sun photometer. Acknowledgment is made to the FGAM (Facility for Ground-Based Atmospheric Measurement), NCAS (National Centre for Atmospheric Science) for the use of the sodar, lidar, and radiosonde units. ECMWF data were provided by the NCAS British Atmospheric Data Centre (BADC, http://badc.nerc.ac.uk/). We thank the Royal Meteorological Institute of Belgium for providing the GERB HR flux data. Marsham is a water@leeds research fellow part funded by ERC grant 257543 “Desert Storms” and NCAS.

References

Allan, R. P., Shine, K. P., Slingo, A., and Pamment, J. A.: The dependence of clear-sky outgoing long-wave radiation on surface temperature and relative humidity, Q. J. Roy. Meteor. Soc., 125, 2103–2126, 1999.

Allen, C. J. T., Washington, R., and Saci, A.: Dust detection from ground-based observations in the summer global dust maximum: Results from Fennec 2011 and 2012 and im-

ACPD
15, 19447–19476, 2015

plications for modeling and field observations, J. Geophys. Res. Atmos., 120, 897–916, doi:10.1002/2014JD022655, 2015.
Balkanski, Y., Schulz, M., Claquin, T., and Guibert, S.: Reevaluation of Mineral aerosol radiative forcings suggests a better agreement with satellite and AERONET data, Atmos. Chem. Phys., 7, 81–95, doi:10.5194/acp-7-81-2007, 2007.
Banks, J. R., Brindley, H. E., Hobby, M., and Marsham, J. H.: The daytime cycle in dust aerosol direct radiative effects observed in the central Sahara during the Fennec campaign in June 2011, J. Geophys. Res. Atmos., 119, 13861–13876, doi:10.1002/2014JD022077, 2014.
Biasutti, M., Sobel, A. H., and Camargo, S. J.: The role of the Sahara low in summertime Sahel rainfall variability and change in the CMIP3 models, J. Climate, 22, 5755–5771, doi:10.1175/2009JCLI2969.1, 2009.
Birch, C. E., Parker, D. J., Marsham, J. H., Copsey, D., and Garcia-Carreras, L.: A seamless assessment of the role of convection in the water cycle of the West African Monsoon, J. Geophys. Res.-Atmos., 119, 2890–2912, doi:10.1002/2013JD020887, 2014.
Bou Karam, D., Flamant, C., Knippertz, P., Reitebuch, O., Pelon, J., Chong, M., and Dabas, A.: Dust emissions over the Sahel associated with the West African monsoon intertropical discontinuity region: a representative case-study, Q. J. Roy. Meteor. Soc., 134, 621–634, doi:10.1002/qj.244, 2008.
Bouniol, D., Couvreux, F., Kamsu-Tamo, P.-H., Leplay, M., Guichard, F., Favot, F., and O'Connor, E. J.: Diurnal and seasonal cycles of cloud occurrences, types, and radiative impact over West Africa, J. Appl. Meteorol. Clim., 51, 534–553, doi:10.1175/JAMC-D-11-051.1, 2012.
Brindley, H. E. and Harries, J. E.: The impact of far i.r. absorption on clear sky greenhouse forcing: sensitivity studies at high spectral resolution, J. Quant. Spectrosc. Ra., 60, 151–180, doi:10.1016/S0022-4073(97)00152-0, 1998.
Charney, C. G.: Dynamics of deserts and drought in the Sahel, Q. J. Roy. Meteor. Soc., 101, 193–202, doi:10.1002/qj.49710142802, 1975.
Chauvin, F., Roehrig, R., and Lafore, J.-P.: Intraseasonal variability of the Saharan heat low and its link with midlatitudes, J. Climate, 23, 2544–2561, doi:10.1175/2010JCLI3093.1, 2010.
Cuesta, J., Marsham, J. H., Parker, D. J., and Flamant, C.: Dynamical mechanisms controlling the vertical redistribution of dust and the thermodynamic structure of the West

ACPD
15, 19447–19476, 2015

Saharan Atmospheric Boundary Layer during Summer, Atmos. Sci. Lett., 10, 34–42, doi:10.1002/asl.207, 2009.
Cuesta, J., Lavaysse, C., Flamant, C., Mimouni, M., and Knippertz, P.: Northward bursts of the West African monsoon leading to rainfall over the Hoggar Massif, Algeria, Q. J. Roy. Meteor. Soc., 136, 174–189, doi:10.1002/qj.439, 2010.
Dee, D. P., Uppala, S. M., Simmons, A. J., Berrisford, P., Poli, P., Kobayashi, S., Andrae, U., Balmaseda, M. A., Balsamo, G., Bauer, P., Bechtold, P., Beljaars, A. C. M., van de Berg, L., Bidlot, J., Bormann, N., Delsol, C., Dragani, R., Fuentes, M., Geer, A. J., Haimberger, L., Healy, S. B., Hersbach, H., Hólm, E. V., Isaksen, L., Kållberg, P., Köhler, M., Matricardi, M., McNally, A. P., Monge-Sanz, B. M., Morcrette, J.-J., Park, B.-K., Peubey, C., de Rosnay, P., Tavolato, C., Thépaut, J.-N., and Vitart, F.: The ERA-Interim reanalysis: configuration and performance of the data assimilation system, Q. J. Roy. Meteor. Soc., 137, 553–597, doi:10.1002/qj.828, 2011.
Dewitte, S., Gonzalez, L., Clerbaux, N., Ipe, A., Bertrand, C., and Paepe, B. D.: The Geostationary Earth Radiation Budget Edition 1 data processing algorithms, Adv. Space Res., 41, 1906–913, doi:10.1016/j.asr.2007.07.042, 2008.
Emmel, C., Knippertz, P., and Schulz, O.: Climatology of convective density currents in the southern foothills of the Atlas Mountains, J. Geophys. Res., 115, D11115, doi:10.1029/2009JD012863, 2010.
Evan, A. T., Flamant, C., Fiedler, S., and Doherty, O.: An analysis of aeolian dust in climate models, Geophys. Res. Lett., 41, 5996–6001, doi:10.1002/2014GL060545, 2014.
Evan, A. T., Flamant, C., Lavaysse, C., Kocha, C., and Saci, A.: Water vapor–forced greenhouse warming over the Sahara Desert and the recent recovery from the Sahelian Drought, J. Climate, 28, 108–123, doi:10.1175/JCLI-D-14-00039.1, 2015.
Garcia-Carreras, L., Marsham, J. H., Parker, D. J., Bain, C. L., Milton, S., Saci, A., Salah-Ferroudj, M., Ouchene, B., and Washington, R.: The impact of convective cold pool outflows on model biases in the Sahara, Geophys. Res. Lett., 40, 1647–1652, doi:10.1002/grl.50239, 2013.
Grams, C. M., Jones, S. C., Marsham, J. H., Parker, D. J., Haywood, J. M., Heuveline, V.: Atlantic inflow to the Saharan heat low: observations and modelling, Q. J. Roy. Meteor. Soc., 136, 125–140, 2010.
Harries, J. E., Russell, J. E., Hanafin, J. A., et al.: The geostationary earth radiation budget project, Q. J. Roy. Meteor. Soc., 86, 945–960, doi:10.1175/BAMS-86-7-945, 2005.

ACPD
15, 19447–19476, 2015

Haywood, J. M., Allan, R. P., Culverwell, I., Slingo, T., Milton, S., Edwards, J., and Clerbaux, N.: Can desert dustexplain the outgoing longwave radiation anomaly over the Sahara during July 2003?, J. Geophys. Res., 110, D05105, doi:10.1029/2004JD005232, 2005.
Heinold, B., Knippertz, P., Marsham, J. H., Fiedler, S., Dixon, N., Schepanski, K., Laurent, B., and Tegen, I.: The role of deep convection and low-level jets for dust emission in summertime West Africa, J. Geophys. Res.-Atmos., 118, 1–16, doi:10.1002/jgrd.50402, 2013.
Holben, B. N., Eck, T. F., Slutsker, I., Tanré, D., Buis, J. P., Setzer, A., Vermote, E., Reagan, J. A., Kaufman, Y. J., Nakajima, T., Lavenu, F., Jankowiak, I., and Smirnov, A.: AERONET – a federated instrument network and data archive for aerosol characterization, Remote Sens. Environ., 66, 1–16, doi:10.1016/S0034-4257(98)00031-5, 1998.
Lavaysse, C., Flamant, C., Janicot, S., Parker, D. J., Lafore, J.-P., Sultan, B., and Pelon, J.: Seasonal evolution of the West African heat low: a climatological perspective, Clim. Dynam., 33, 313–330, 2009.
Lavaysse, C., Flamant, C., Janicot, S., and Knippertz, P.: Links between African easterly waves, midlatitude circulation and intraseasonal pulsations of the West African heat low, Q. J. Roy. Meteor. Soc., 136, 141–158, 2010a.
Lavaysse, C., Flamant, C., and Janicot, S.: Regional-scale convection patterns during strong and weak phases of the Saharan heat low, Atmos. Sci. Lett., 11, 255–264, doi:10.1002/asl.284, 2010b.
Marsham, J. H., Parker, D. J., Grams, C. M., Taylor, C. M., and Haywood, J. M.: Uplift of Saharan dust south of the inter-tropical discontinuity, J. Geophys. Res.-Atmos., 113, D21102, doi:10.1029/2008JD009844, 2008.
Marsham, J. H., Knippertz, P., Dixon, N., Parker, D. J., and Lister, G. M. S.: The importance of the representation of deep convection for modeled dust-generating winds over West Africa during summer, Geophys. Res. Lett., 38, L16803, doi:10.1029/2011GL048368, 2011.
Marsham, J. H., Hobby, M., Allen, C. J. T., Banks, J. R., Bart, M., Brooks, B. J., Cavazos-Guerra, C., Engelstaedter, S., Gascoyne, M., Lima, A. R., Martins, J. V., McQuaid, J. B., O'Leary, A., Ouchene, B., Ouladichir, A., Parker, D. J., Saci, A., Salah-Ferroudj, M., Todd, M. C., and Washington, R.: Meteorology and dust in the central Sahara: observations from Fennec supersite-1 during the June 2011 Intensive Observation Period, J. Geophys. Res.-Atmos., 118, 4069–4089, doi:10.1002/jgrd.50211, 2013a.
Marsham, J. H., Dixon, N., Garcia-Carreras, L., Lister, G. M. S., Parker, D. J., Knippertz, P., and Birch, C. E.: The role of moist convection in the West African monsoon system – insights

ACPD
15, 19447–19476, 2015

from continental-scale convection-permitting simulations, Geophys. Res. Lett., 40, 1843–1849, doi:10.1002/grl.50347, 2013b.
Martin, E. R. and Thorncroft, C. D.: The impact of the AMO on the West African monsoon annual cycle, Q. J. Roy. Meteor. Soc., 140, 31–46, doi:10.1002/qj.2107, 2014.
Martin, E. R., Thorncroft, C. D., and Booth, B. B.: The multidecadal Atlantic SST–Sahel rainfall teleconnection in CMIP5 simulations, J. Climate, 27, 784–805, doi:10.1175/JCLI-D-13-00242.1, 2014.
Parker, D. J., Thorncroft, C. D., Burton, R. R., and Diongue-Niang, A.: Analysis of the African easterly jet, using aircraft observations from the JET2000 experiment, Q. J. Roy. Meteor. Soc., 131, 1461–1482, doi:10.1256/qj.03.189, 2005.
Peyrillé, P. and Lafore, J.-P.: An idealized two-dimensional framework to study the West African monsoon. Part II: Large-scale advection and the diurnal cycle, J. Atmos. Sci., 64, 2783–2803, doi:10.1175/JAS4052.1, 2007.
Roberts, A., Marsham, J. H., and Knippertz, P.: Disagreements in low-level moisture between (re)analyses over summertime West Africa, Mon. Weather Rev., 143, 1193–1211, doi:10.1175/MWR-D-14-00218.1, 2015.
Ryder, C. L., Highwood, E. J., Rosenberg, P. D., Trembath, J., Brooke, J. K., Bart, M., Dean, A., Crosier, J., Dorsey, J., Brindley, H., Banks, J., Marsham, J. H., McQuaid, J. B., Sodemann, H., and Washington, R.: Optical properties of Saharan dust aerosol and contribution from the coarse mode as measured during the Fennec 2011 aircraft campaign, Atmos. Chem. Phys., 13, 303–325, doi:10.5194/acp-13-303-2013, 2013.
Ryder, C. L., McQuaid, J. B., Flamant, C., Washington, R., Brindley, H. E., Highwood, E. J., Marsham, J. H., Parker, D. J., Todd, M. C., Banks, J. R., Brooke, J. K., Engelstaedter, S., Estellés, V., Formenti, P., Garcia-Carreras, L., Kocha, C., Marenco, F., Rosenberg, P., Sodemann, H., Allen, C. J. T., Bourdon, A., Bart, M., Cavazos-Guerra, C., Chevaillier, S., Crosier, J., Darbyshire, E., Dean, A. R., Dorsey, J. R., Kent, J., O'Sullivan, D., Schepanski, K., Szpek, K., and Woolley, A.: Advances in understanding mineral dust and boundary layer processes over the Sahara from Fennec aircraft observations, Atmos. Chem. Phys. Discuss., 15, 199–290, doi:10.5194/acpd-15-199-2015, 2015.
Stein, T. H. M., Parker, D. J., Delanoë, J., Dixon, N. S., Hogan, R. J., Knippertz, P., and Marsham, J. H.: Vertical cloud structure for the West African monsoon: a four-year climatology using CloudSat and CALIPSO, J. Geophys. Res. Atmos., 116, D22205, doi:10.1029/2011JD016029, 2011.

ACPD
15, 19447–19476, 2015

Sultan, B. and Janicot, S.: The West African Monsoon dynamics, Part II: The "preonset" and "onset" of the summer monsoon, J Climate, 16, 3407–3427, 2003.

Thorncroft, C. D. and Blackburn, M.: Maintenance of the African easterly jet, Q. J. Roy. Meteor. Soc., 125, 763–786, doi:10.1002/qj.49712555502, 1999.

Todd, M. C., Allen, C. J. T., Bart, M., Bechir, M., Bentefouet, J., Brooks, B. J., Cavazos-Guerra, C., Clovis, T., Deyane, S., Dieh, M., Engelstaedter, S., Flamant, C., Garcia-Carreras, L., Gandega, A., Gascoyne, M., Hobby, M., Kocha, C., Lavaysse, C., Marsham, J. H., Martins, J. V., McQuaid, J. B., Ngamini, J. B., Parker, D. J., Podvin, T., Rocha-Lima, A., Traore, S., Wang, Y., and Washington, R.: Meteorological and dust aerosol conditions over the Western Saharan region observed at Fennec supersite-2 during the Intensive Observation Period in June 2011, J. Geophys. Res.-Atmos., 118, 8426–8447, doi:10.1002/jgrd.50470, 2013.

Washington, R., Flamant, C., Parker, D. J., Marsham, J., McQuaid, J., Brindley, H., Todd, M., Highwood, E., Ryder, C., Chaboureau, J.-P., Kocha, C., Bechir, M., and Saci, A.: Fennec – the Saharan Climate System, CLIVAR Exchanges, 17, 31–32, 2012.

Xue, Y., De Sales, F., Lau, W. K.-M., Boone, A., Feng, J., Dirmeyer, P., Guo, Z., Kim, K.-M., Kitoh, A., Kumar, V., Poccard-Leclercq, I., Mahowald, N., Moufouma-Okia, W., Pegion, P., Rowell, D. P., Schemm, J., Schubert, S. D., Sealy, A., Thiaw, W. M., Vintzileos, A., Williams, S. F., and Wu, M.-L. C.: Intercomparison and analyses of the climatology of the West African Monsoon in the West African Monsoon Modeling and Evaluation project (WAMME) first model intercomparison experiment, Clim. Dynam., 35, 3–27, doi:10.1007/s00382-010-0778-2, 2010.

Yang, E.-S., Gupta, P., and Sundar, A. C.: Net radiative effect of dust aerosols from satellite measurements over Sahara, Geophys. Res. Lett., 36, L18812, doi:10.1029/2009GL039801, 2009.

ACPD
15, 19447–19476, 2015

Table 1. Gradients of best-fit straight lines for listed relationships, values in [ ] are normalised by standard deviation of TCWV or AOD. Values in ( ) are correlation coefficients (bold values are significant at 90 % level). For ERA-I observed AODs are used. Standard deviation in TCWV in ERA-I = 4.7 kg m^{-2} (4.5 for "All data"). For observations 4.7 kg m^{-2} (4.4 for "All data"). Standard deviation in AOD for observations is 0.68 (0.65 in "All data").

	Observations		ERA-I	
	Good surface data	All data	Good surface data	All data
TCWV : AOD (kg m^{-2})	0.04 (**0.29**)	0.04 (**0.30**)	0.02 (0.16)	0.02 (0.14)
AOD : TOA Net (W m^{-2})	5.3 [3.6] (**0.26**)	3.5 [2.3] r (0.17)	1.7 (0.12)	0.33 (0.02)
AOD : TOA Net LW (W m^{-2})	10.5 [7.2] (**0.33**)	8.5 [5.5] (**0.26**)	2.4 (0.12)	1.0 (0.05)
AOD : TOA Net SW (W m^{-2})	−5.2 [−3.6] (**−0.28**)	−5.0 [−3.3] (**−0.26**)	−0.72 (−0.07)	−0.70 (−0.06)
TCWV : TOA Net (W kg^{-1})	2.2 [10.4] (**0.74**)	2.1 [9.2] (**0.68**)	1.3 (**0.66**)	1.4 (**0.66**)
TCWV : TOA Net LW (W m^{-2} kg^{-1} m^2)	3.2 [15.0] (**0.68**)	3.0 [13.3] (**0.63**)	1.8 (**0.61**)	2.0 (**0.65**)
TCWV : TOA Net SW (W kg^{-1})	−0.98 [−4.6] (**−0.36**)	−0.9 [−4.1] (**−0.33**)	−0.48 (**−0.30**)	−0.49 (**−0.30**)
TOA Net SW : TOA Net LW	−1.38 (**−0.80**)	−1.35 (**−0.79**)	−1.44 (**−0.78**)	−1.39 (**−0.72**)
AOD : Surface Net (W m^{-2})	−13.1 [−9.0] (**−0.70**)	–	3.4 (**0.34**)	3.2 (**0.31**)
AOD : Surface Net SW (W m^{-2})	−31.9 [−21.8] (**−0.87**)	–	−1.6 (−0.12)	−1.7 (−0.12)
AOD : Surface Net LW (W m^{-2})	20.7 [14.2] (**0.81**)	–	5.0 (**0.28**)	4.9 (**0.27**)
TCWV : Surface Net (W kg^{-1})	−0.20 [−0.96] (−0.07)	–	0.76 (**0.53**)	0.85 (**0.57**)
TCWV : Surface Net LW (W kg^{-1})	2.0 [9.3] (**0.54**)	–	2.2 (**0.84**)	2.2 (**0.85**)
TCWV : Surface Net SW (W kg^{-1})	−1.8 [−8.2] (**−0.33**)	–	−1.4 (**−0.69**)	−1.4 (**−0.68**)
Surface Net SW : Surface Net LW	−0.61 (**−0.88**)	–	−1.1 (**−0.83**)	−1.1 (**−0.82**)
AOD : Atmospheric Net (W m^{-2})	18.5 [12.1] (**0.62**)	–	−1.75 (−0.13)	−2.9 (0.21)
AOD : Atmospheric Net LW (W m^{-2})	−10.2 [−6.7] (**−0.41**)	–	−2.65 (−0.18)	−3.9 (**−0.26**)
AOD : Atmospheric Net SW (W m^{-2})	26.7 [17.5] (**0.93**)	–	0.91 (0.13)	1.0 (0.15)
TCWV : Atmospheric Net (W kg^{-1})	2.4 [10.7] (**0.56**)	–	0.51 (**0.26**)	0.54 (**0.27**)
TCWV : Atmospheric Net LW (W kg^{-1})	1.2 [5.4] (**0.34**)	–	−0.41 (−0.20)	−0.36 (−0.17)
TCWV : Atmospheric Net SW (W kg^{-1})	0.78 [3.4] (**0.19**)	–	0.91 (**0.93**)	0.90 (**0.91**)
Atmos Net SW : Atmos Net LW	−0.39 (**−0.45**)	–	−0.73 (**−0.35**)	−0.79 (**−0.36**)

ACPD
15, 19447–19476, 2015

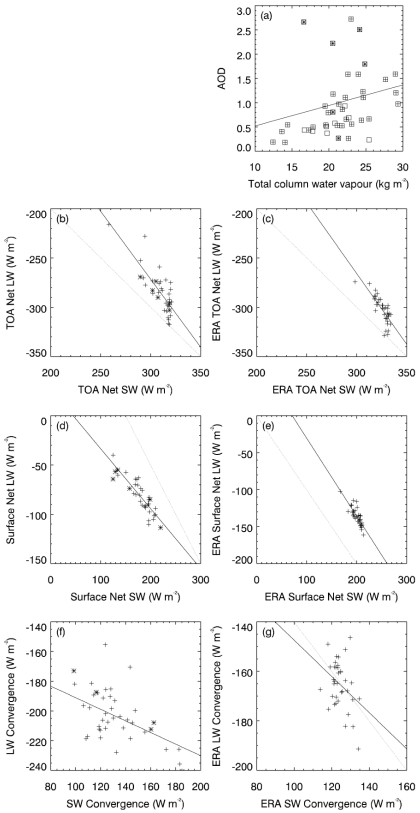

Figure 1. Daily means of: **(a)** TCWV and AOD, **(b, c)** TOA fluxes, **(d, e)** surface fluxes, **(f, g)** inferred atmospheric heating. Values are observations except **(c, e, g)** are for ERA-I. Pluses show days with complete surface data, stars days with some interpolation (see Sect. 2). In **(a)** squares show all data points (including days with no surface-flux data), **(b–g)** show only days where surface data are available.

ACPD
15, 19447–19476, 2015

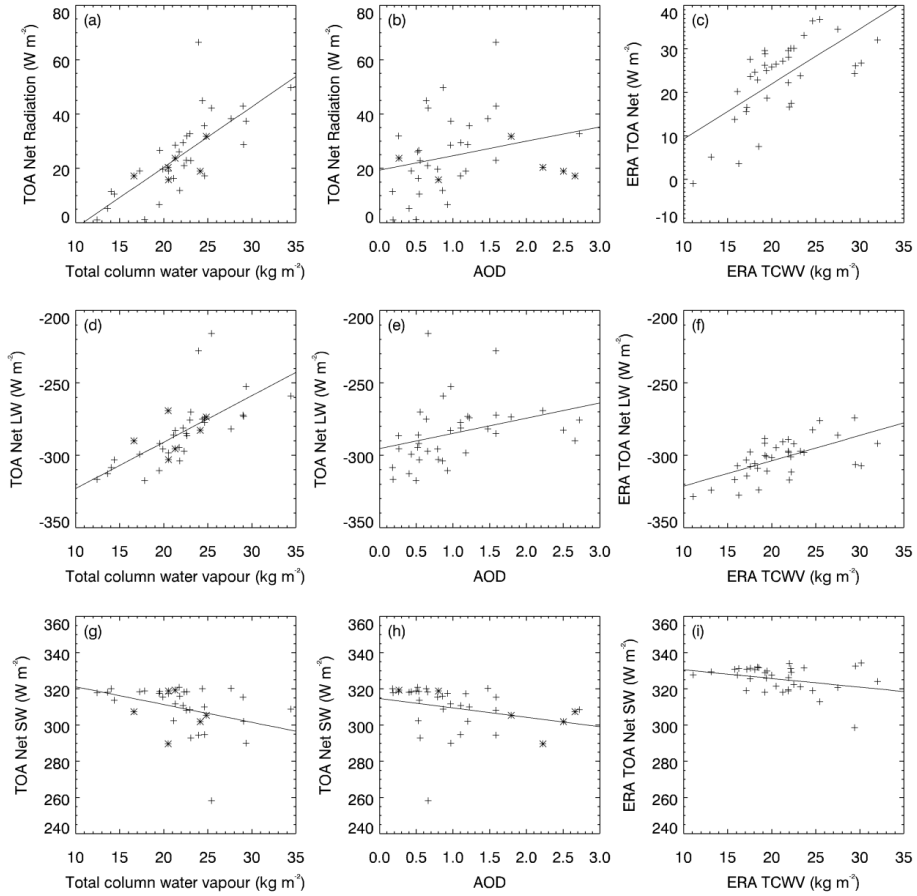

Figure 2. TOA fluxes, with symbols as in Fig. 1b–g, showing means for days with surface data.

ACPD
15, 19447–19476, 2015

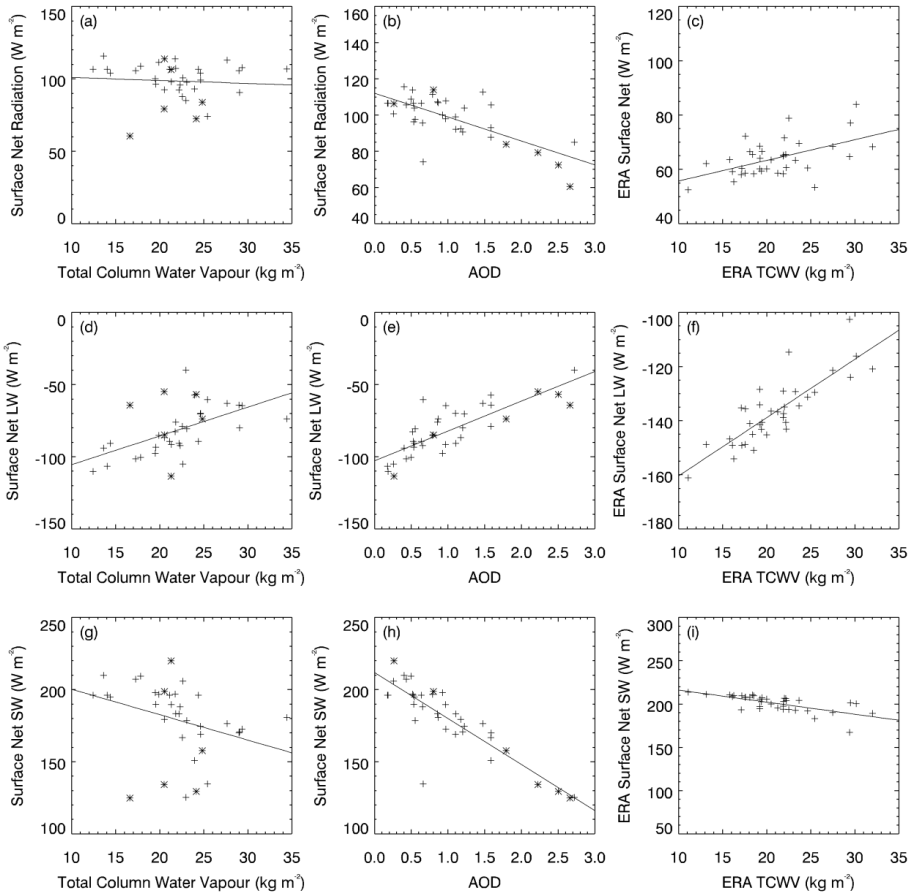

Figure 3. As Fig. 2, but for surface fluxes.

ACPD
15, 19447–19476, 2015

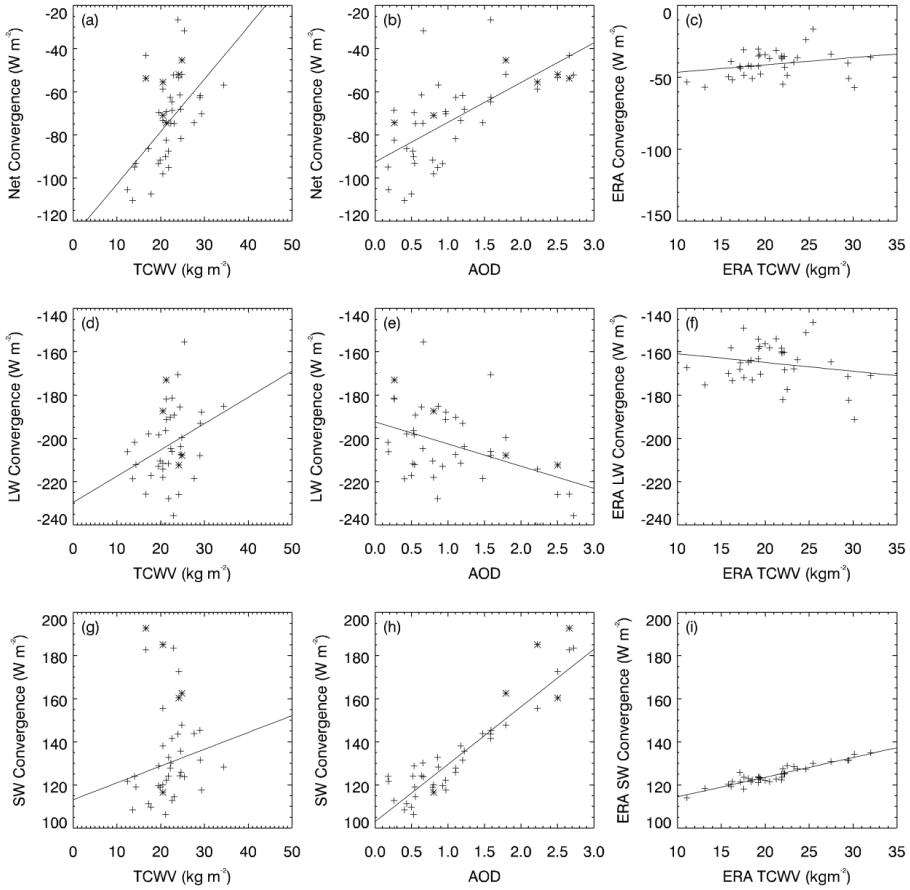

Figure 4. As Fig. 2, but for inferred atmospheric heating (TOA flux minus surface flux).

ACPD
15, 19447–19476, 2015

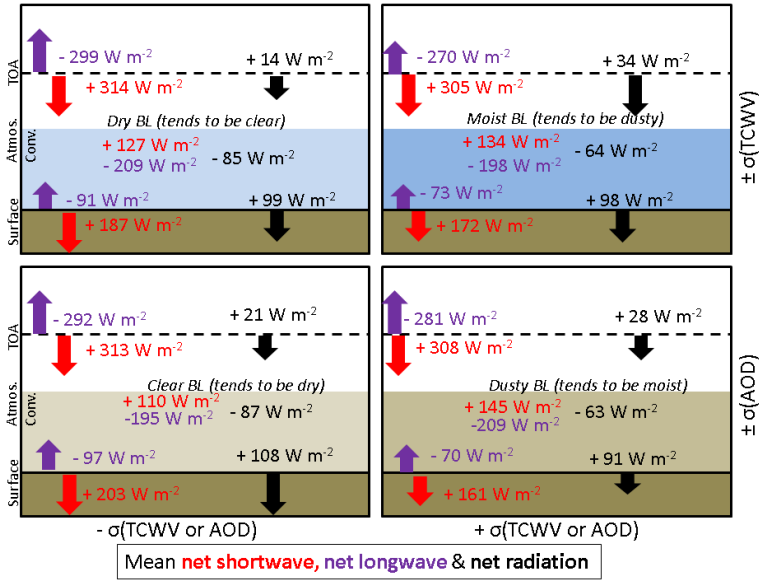

Figure 5. Schematic showing net radiation and implied tropospheric radiative heating, in situations where either TCWV (top row) or AOD (bottom row) is perturbed by plus or minus one standard deviation away from their mean state (right and left columns respectively). Moist atmospheres tend to be dusty and visa-versa. Red numbers show net shortwave, purple show net longwave and black show net radiation. TOA and surface heating are shown by plus signs with downward arrows. Values are shown at surface, TOA and for inferred atmospheric radiative heating ("Atmos. Conv."). Variance in TCWV has the dominant effect on net TOA radiation, while variance in AOD has the dominant effect on net surface radiation. Both TCWV and AOD are important for atmospheric heating rates.

ACPD
15, 19447–19476, 2015